Journal of Non-Newtonian Fluid Mechanics 243 (2017) 16–26

Contents lists available at ScienceDirect

Journal of Non-Newtonian Fluid Mechanics

journal homepage: www.elsevier.com/locate/jnnfm

Ink transfer of non-Newtonian fluids from an idealized gravure cell: The effect of shear and extensional deformation

Sunilkumar Khandavalli, Jonathan P. Rothstein*

Mechanical and Industrial Engineering, University of Massachusetts Amherst, MA 01003 USA

ARTICLE INFO

Article history:
Received 17 August 2016
Revised 23 December 2016
Accepted 17 February 2017
Available online 16 March 2017

Keywords:
Gravure printing
Viscoelasticity
Shear thickening
Colloids
Extensional rheology
Shear rheology
Roll-to-roll

ABSTRACT

In the presented study, we have investigated the effect of a complex flow field consisting of a combination of both shear and extensional deformation on the liquid transfer from an idealized gravure cell. The study was conducted for two classes of non-Newtonian fluid; a shear and extensional thickening nanoparticle dispersion and a extensional thickening viscoelastic polymer solution with a constant shear viscosity. The shear thickening fluid was a dispersion of fumed silica nanoparticles in polypropylene glycol and the viscoelastic fluid was a solution of polyethylene oxide (PEO) in water. The idealized gravure printing experiments were conducted using a combination of linear servo motor used to impose an extensional flow and a rotational servo motor to impose a shear flow during pickout. The fluid pickout from the gravure cell was studied as a function of the magnitude of the extensional and shear deformation rates. The fluid filament interface profile evolution during the pickout process was examined using a high speed camera. For the shear thickening fluid, the pickout resulting from a pure extensional flow field was found to be enhanced compared to Newtonian fluids at moderate velocities, resulting from the extensional thickening of the fluid. However, at large stretching velocities the pickout was found to decay dramatically due to extensional thinning of the fluid at large extension rates. The pickout behavior of the shear thickening fluid resulting from a pure shear field was found to exhibit a qualitatively similar trend to that of the extensional pickout although the pickout fraction was significantly smaller. Superposition of shear and extensional flow was found to initially improve pickout by driving the overall deformation rate higher and introducing an asymmetry in the gravure cell dewetting. At large rates, shear negatively affected pickout by causing an early onset of extensional thinning. In viscoelastic fluids, thickening of the extensional viscosity was found to enhance both the pure shear-induced pickout as well as the pure extensional-induced fluid pickout, with the shear-induced pickout relatively smaller compared to the extensional-induced pickout. For superimposed shear and extensional deformation, an enhancement in the fluid pickout was observed at certain velocity regimes, likely associated with the asymmetric dewetting from the gravure cavity wall assisted by the superimposed flows.

1. Introduction

Roll-to-roll coating and printing of flexible substrates is a technology of great industrial and commercial importance due to its low cost and high throughput [1,2]. This technology enables the fabrication of thin organic, inorganic and mixed organic/inorganic films with nanoscale patterns at high resolution for devices in wide applications such as, solar cells, thin film transistors, organic light emitting diodes, biosensors and biodevices [3–8]. Gravure printing is a roll-to-roll processing technique used to coat/print thin films less than 50 μm for a wide variety of applications in high volumes such as magazines, packaging, flexible electronics, greeting cards and tapes [9–12]. In the gravure printing process, a roller with desired engraving, typically in tens of microns dimensions, is passed through an ink reservoir and the excess is metered off by passing by a doctor blade. The ink from the cavities is then deposited on to the substrate held by another roller at high speeds of up to 10 m/s.

During the ink transfer process, a liquid bridge is formed and stretched between the gravure cell and web, as the ink is deposited onto the substrate. The liquid bridge experiences a combination of shear, extension and rotation due to relative motion between the gravure cell and web [13,14]. The stability and breakup dynamics of the liquid bridge during the ink transfer can significantly affect the quality of the print or coated film. Partial emptying of the cavities or the formation of satellite drops can negatively impact the qual-

* Corresponding author.
E-mail address: rothstein@ecs.umass.edu (J.P. Rothstein).

http://dx.doi.org/10.1016/j.jnnfm.2017.02.005
0377-0257/

ity and the efficiency of the printing process [15]. As with gravure printing, the dynamics of the liquid bridge are strongly relevant in other applications such as contact drop dispensing [16], float-zone crystallization [17] and oil recovery [18]. As a result, the dynamics, stability and breakup of the liquid bridge have been widely studied [16,18–22]. Numerous studies, both experimental and numerical, have been performed to better understand the dynamics of a liquid bridge uniaxially stretched between two flat plates [23–26], as well between a flat plate and a cavity [27–30]. There have also been numerical and experimental studies on ink transfer behavior in gravure printing considering pure shear flow [31–33] as well as some which imposed a combination of shear and extensional motion of the liquid bridge [34,35]. Additionally, a few considering the effect of the rotation of the gravure cavity as the liquid is applied to the moving web by the rotating gravure roller [13,35].

Printing fluids often are non-Newtonian, as many inks contain large concentrations of particles and polymer additives [7,12,36]. Only a few recent studies, some experimental [10,37] and some computations [37–40], have reported on the behavior of non-Newtonian fluids during gravure printing. These studies include measurements on non-Newtonian fluid with rheological properties ranging from shear-thinning [38] to viscoelasticity [10,38–40] and more recently to shear-thickening [37]. Ahn et al. [39] examined the influence of elasticity through numerical computations using Oldroyd-B model and observed significant differences in the velocity field and pressure distribution in the cavity between viscoelastic and Newtonian fluids. Sankaran and Rothstein [10] conducted experimental investigation using polyethylene oxide (PEO) fluids to study the impact of viscoelasticity, gravity and gravure cell design on the fluid transfer in gravure printing. Filament stabilization due to elasticity was found to enhance or worsen the fluid removal, depending on whether the fluid removal direction is aligned with or opposite to the direction of gravity. Computational studies later by Lee et al. [40] on the influence of viscoelasticity in gravure printing using FENE-P constitutive model were in excellent agreement with experiments [10]. Their computations were able to extend beyond the parameters of the experiments to investigate a larger viscoelastic parameter space. Khandavalli et al.[37] studied gravure printing behavior of shear-thickening nanoparticle dispersions, through a combination of experiments and computations. Beyond a critical stretch rate, shear-thickening of the fluid was manifested by the formation of long stable filaments, which was found to enhance gravitational drainage during pickout. Beyond a second critical stretch rate, shear and extensional-thinning were found to induce conical profile evolution and resulted in a pickout fraction insensitive to the stretch rate.

Most studies which have focused on gravure printing of non-Newtonian fluids have modeled liquid bridge stretching during ink transfer processes as a purely extensional flow [10,27–30,37,38,40]. In addition to extensional flow, in the real gravure printing process, the liquid bridge also experiences rotation and strong shear deformation due to relative motion between the top and bottom rollers. Unfortunately, only a few studies exist on gravure printing considering shear deformation of the liquid bridge during ink transfer and most have all been for Newtonian fluids [13,31,35,41,42]. These studies using Newtonian fluids have found that, for a gravure printing process modeled as pure shear, the fluid pickout from gravure cells decreased with increasing capillary number at low to moderate capillary numbers [13,31,35,41,42]. This is opposite to the trend observed in the pickout process modeled as pure extension [10,13,28,34,42]. The driving mechanism for the shear pickout at low capillary number in shear has been attributed to a lateral capillary pressure gradient developed due to the non-symmetric meniscus curvature evolved in shear motion [13,31]. Capillary number is given as, $\mathrm{Ca} = \eta V/\sigma$, where η, σ, and V are fluid viscosity, surface tension and stretch speeds. Campana and Carvalho [13] conducted a computational study on fluid pickout from gravure cells for a wide capillary number space, $0.01 < \mathrm{Ca} < 1$, while imposing the complete roll-to-roll kinematics of the plate, including shear, extension and rotation. Through their simulations, they were able to observe the free surface profile evolution and contact line motion. The results of their simulations showed a non-linear pickout behavior with increasing capillary number which was due in large part to the contact line mobility. At low capillary numbers, $\mathrm{Ca} < 0.1$, the lateral contact line mobility resulted in a large pickout and a flow dominated by the shear and rotational motion of the gravure cell. Whereas, at large capillary numbers, contact line motion pinning resulted in a reduction in the pickout and a flow dominated by extensional motion of the top plate.

Only one study on non-Newtonian fluid case considering shear motion in gravure printing process has been reported recently by Chung and Kumar [43], where they conduct a computational study of the pickout behavior from model gravure cells for viscoelastic fluids cases considering a combination of horizontal and vertical substrate motion. For a pure horizontal substrate motion, the pickout was found to be improved for a viscoelastic case compared to a Newtonian fluid, due to a large first normal stress gradient generated near the downstream corner of the cavity. When an extensional motion superimposed over horizontal motion of the substrate, the pickout was found to be improved, with a stronger enhancement of the pickout fraction for viscoelastic fluids as compared to a Newtonian fluid.

Previously, our research group has conducted studies on the effect of viscoelasticity [10] and shear-thickening [37] on the ink transfer behavior in gravure printing, modeling the ink transfer process as pure extensional deformation of the liquid bridge. To extend the previous studies, in this paper we present the investigation on the effect of shear deformation, as well as a complex combination of shear and extensional deformation on the liquid bridge during the ink transfer process in gravure printing. The study is presented for both constant shear viscosity viscoelastic fluids and shear-thickening inelastic nanoparticle dispersions. The test fluids were chosen to be the same as the previous studies so that conclusions could be more easily drawn. The test fluids consisted of an aqueous polyethylene oxide (PEO) solution and fumed silica nanoparticle dispersion in polypropylene glycol (PPG). The amount of ink transferred from an idealized gravure cell was studied over a wide range of extensional and shear deformation rates chosen to probe the test fluids at rates capable of engaging shear thickening/thinning and viscoelastic effects.

2. Methods and materials

2.1. Gravure printing experimental setup

In our experiments, the gravure printing process was modeled as a combination of uniaxial extension and shear deformation of the liquid bridge during the ink transfer process. The experimental set-up was similar to that used in our previous study [10], but with a slight modification of the set-up, as shown in Fig. 1. Uniaxial extensional motion on the liquid bridge was imposed using a modified version of a filament stretching extensional rheometer, where the top flat aluminum plate was replaced with an inverted gravure cell. To impose shear deformation, the bottom flat plate was attached to a servo-motor through a rotating fixture. Both the linear-motor and the servo-motor were computer-controlled to simultaneously impose the desired shear and extensional velocities. The truncated cone shaped gravure cell (cavity) was fabricated by casting PDMS (Sylgard 184) onto a negative mold of the cavity machined into aluminum. The cavity has a sidewall angle of $\alpha = 75^\circ$ from horizontal, radius of $R = 2.5$ mm and a depth of $h = 1$ mm. The real gravure rollers have cavity features that are

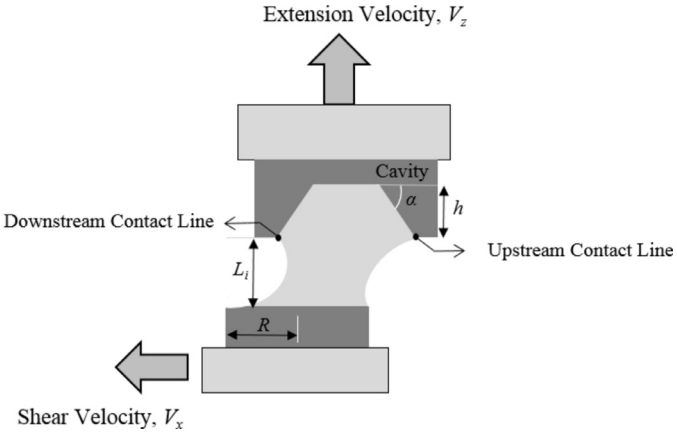

Fig. 1. Schematic diagram of experimental setup used for idealized gravure cell study.

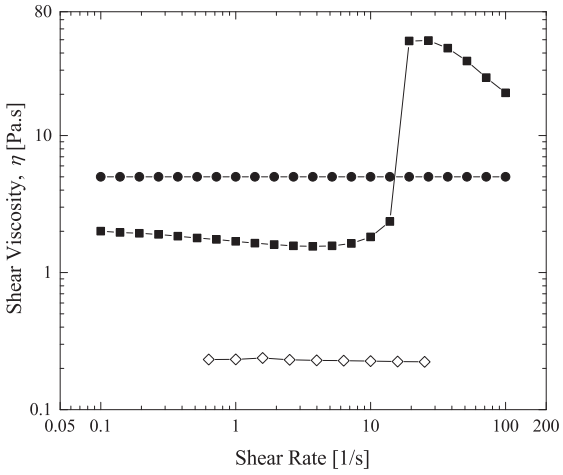

Fig. 2. Steady shear viscosity as a function of shear rate. The data include: a) (■) 13Si-PPG, (◇) 8M PEO and (○) Silicone oil.

typically ten to hundred microns in order. Here the cavity dimensions were scaled for the convenience of a lab scale study. The result is that gravity is more important in our experiments than in a true gravure printing process [40]. A cylindrical fluid filament was held between the plate and cavity at an initial aspect ratio of $L_i/R = 0.3$, where L_i is the separation. The initial separation between cavity and the plate which is larger than in a real printing process, was chosen for convenience of the experiments to make massing the fluid easier. There have been studies that have found a larger amount of ink transfer for smaller cavity depths [10], initial liquid bridge aspect ratios and initial fluid volume [31].

In pure extensional flow experiments, the top cavity was separated at different extensional velocities ranging from 0.1 to 200 mm/s to a final aspect ratio of $L_f / R \sim 32$. At these aspect ratios, the filaments survived in only a few cases. In pure shear flow experiments, the bottom flat plate was separated with shear velocities ranging from 1 to 90 mm/s. The imposed speeds corresponded roughly to speeds experienced during gravure printing. The inertia effects were negligible in these tests as the Reynolds numbers were all very low, $\mathrm{Re} = D_0 V \rho/\eta_0 < 5 \times 10^{-2}$ Here D_0 and V are the characteristic diameter and velocity, while ρ and η_0 are the fluid density and zero-shear-rate viscosity. The filament profile evolution during the stretching, shearing and the breakup process was examined using a high-speed video camera (Vision Research, Phantom 4.6). The initial and final mass of the fluid in the cavity was measured using a high precision mass balance (Mettler AC 100). The pickout fraction is defined as, $\phi = m/M$, where m is mass transferred from the gravure cell to the flat plate and M is the total mass of the fluid. The uncertainty in the experimentally measured values of pickout was calculated to be below 2%.

Here we present the study only for the gravure cavity-on-top configuration and have not presented the study for the cavity-on-bottom configuration as was done in Sankaran and Rothstein [10] due to experimental difficulties in accurately quantifying the pickout values, particularly at velocity regimes where elongated fluid filaments were observed. Under shear deformation, as the bottom plate is separated horizontally from the top plate, it does not remain vertically inline with top plate. As a result, when long filament evolved and break-up, some fraction of fluid did not remain in the bottom plate, but was lost to the experimental stage area. This fraction of the fluid was difficult to quantify. As a result, in this orientation deposition volume is easy to quantify, but pickout volume is not. For that reason, we focused on the cavity-on-top configuration.

As seen in Fig. 1, the bottom plate was a cylindrical rod with a diameter of $D = 5$ mm. In all experiments presented here, the contact line of the liquid bridge was pinned at the edge of the rod. It should be noted that in a real gravure printing process, the contact line of the liquid bridge is not forcibly pinned but is free to move along a long flat substrate. In reality, however, either the fluid viscosity or the wettability of the substrate inhibit contact line motion. Clearly the spreading of the ink along the substrate is typically not a desired result for printing discrete patterns.

2.2. Test fluids

The shear thickening test fluid was formulated from 13 wt% fumed silica nanoparticles (Aerosil @380, Evonik Industries; primary particle diameter 7 nm, specific surface area 380 m^2/g) dispersed in polypropylene glycol (PPG) (Aldrich Chemicals, average M.W 1000 g/mol). In the text, this fluid will be given the acronym 13Si-PPG. The shear thickening fluid sample was prepared according to procedure reported in Khandavalli et al. [37]. The viscoelastic test fluid formulated was polyethylene oxide (PEO) (Aldrich Chemicals) solution dissolved in water. The PEO was mixed with water and stirred for 24 h to obtain a homogenous solution. The viscoelastic fluid contained 20 wt% of 2×10^4 g/mol PEO to viscosify the solvent along with an additional 0.16 wt% of a high molecular weight 8×10^6 g/mol PEO to make the fluid elastic. In the text, this fluid will known to be as 8M PEO. The model Newtonian fluid used was a silicone oil with a viscosity of 5 Pa.s (RT5000, CANNON Instrument Co.). The surface tension of the shear thickening fluid, viscoelastic fluid and the Newtonian fluid were measured to be 30 mN/m, 58 mN/m and 20 mN/m respectively using a pendant drop tensiometer (Dataphysics OCA 15plus) [10].

2.2.1. Shear rheology

The steady shear rheology was probed using a stress-controlled TA DHR-3 rheometer using a 40 mm aluminum parallel-plate geometry at a constant temperature of 25 °C with a solvent trap to prevent evaporation. The samples were pre-sheared to erase any shear history during sampling preparation and handing [44,45]. After pre-shearing, each of the sample was were allowed to rest for 4 min to reach equilibrium. Steady shear viscosity measurements were conducted in the shear rate range between $0.1\,s^{-1} \leq \dot{\gamma} \leq 100\,s^{-1}$.

The shear rheology measurements for the three test fluids, shear thickening fluid (13Si-PPG), viscoelastic fluid (8M PEO) and the Newtonian silicone oil, are shown in Fig. 2. The shear thickening fluid at low shear rates exhibited a shear thinning behavior, resulting from the formation of strings of particles aligned along

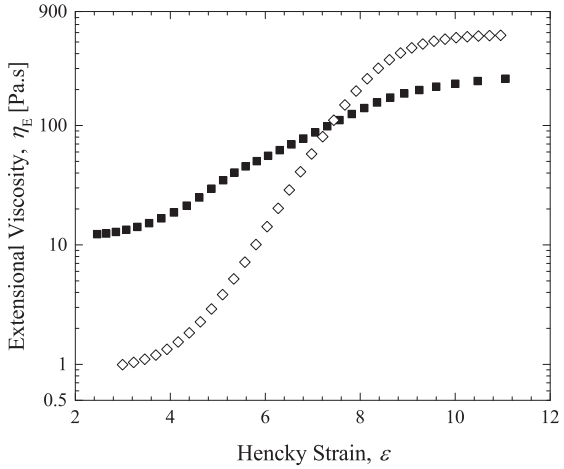

Fig. 3. Apparent extensional viscosity as a function of Hencky strain. The data include: (■) 13Si-PPG and (◇) 8M PEO.

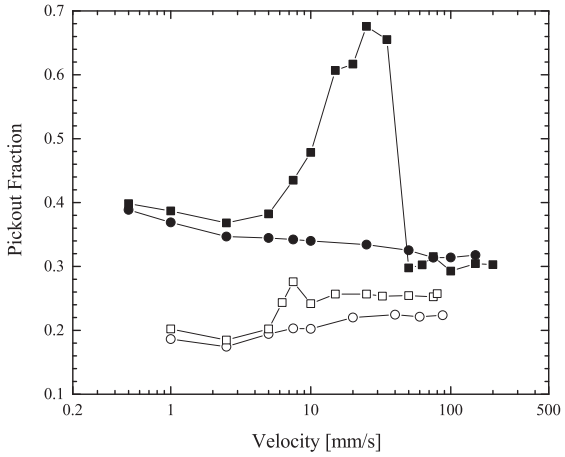

Fig. 4. Pickout fraction as a function of extensional velocity, V_z (filled symbols) and shear velocity, V_x (hollow symbols). The data include: (■) 13Si-PPG and (○) silicone oil.

the direction of shear fields [46]. At a critical shear rate of approximately $\dot{\gamma} = 10\ \ s^{-1}$, the fluid viscosity was found to exhibit sudden shear thickening by more than an order of magnitude from 2 Pa.s to 50 Pa.s. The mechanism for the shear-thickening behavior of these nanoparticles has been attributed to the formation of large hydrodynamic-induced clusters of nanoparticles [46]. With further increase in the shear rate, the fluid was observed to shear-thin. The thinning at larger shear rates has been associated with yielding of the hydrocluster microstructure. The steady shear response of both the viscoelastic fluid and the silicone oil exhibited a constant shear viscosity of 0.2 Pa.s and 5 Pa.s respectively.

2.2.2. Extensional rheology

The extensional viscosity of the three test fluids was measured using a capillary breakup extensional rheometer (CaBER). CaBER is typically used to characterize less viscous fluids making it perfectly suited for 8M PEO [47–51]. The CaBER measurements presented here were performed using a high-speed capillary breakup extensional rheometer designed and developed specifically for these experiments. In CaBER experiments, a cylindrical liquid bridge is created between two circular plates and is stretched from an initial length, L_0, to a final length, L_f, at a constant velocity. Once the stretch is stopped, the capillary thinning of the liquid bridge formed between the two end plates results in a uniaxial extensional flow that can be used to measure extensional viscosity and extensional relaxation time. By monitoring the evolution of the filament diameter as a function of time, the extension rate, $\dot{\varepsilon}$, of the fluid filament can be calculated as

$$\dot{\varepsilon} = -\frac{2}{R_{mid}(t)}\frac{dR_{mid}(t)}{dt}. \quad (1)$$

The apparent extensional viscosity, η_E, can be calculated by applying a force balance between capillary stresses and the viscous and elastic tensile stresses within the fluid filament ignoring inertia [50,51] as

$$\eta_{E.app} = \frac{\sigma/R_{mid}(t)}{\dot{\varepsilon}} = \frac{-\sigma}{dD_{mid}(t)/dt}. \quad (2)$$

The initial and final aspect ratios of the liquid bridge were set as, $\Lambda_0 = 1$ and $\Lambda_f = 3$. Where $\Lambda_0 = L_0/R_0$ and L_0 is the initial separation between the plates.

The apparent extensional viscosity, η_E, as a function of Hencky strain, ε, for the shear thickening fluid and the viscoelastic fluid is shown in Fig. 3. For both the fluids, the apparent extensional viscosity increases with increasing Hencky strain indicating extensional thickening of the fluids. At low Hencky strains, the Trouton ratio, $Tr = \eta_{E,0}/\eta_0$, for both fluids is approximately three, $Tr \approx 3$. The steady-state Trouton ratio, $Tr = \eta_{E,\infty}/\eta_0$, of 13Si-PPG and 8M PEO were found to be approximately $Tr = 50$ and $Tr = 2500$, respectively, indicating significant extensional thickening of both the test fluids. These measurements are consistent with previous measurements of similar systems in the literature [37,52]. Fitting the 8M PEO data to an Oldroyd-B model, an extensional relaxation of $\lambda_E = 0.2$ s was calculated.

3. Results and discussion

3.1. Ink transfer behavior of a shear thickening fluid

3.1.1. Effect of extension

The fraction of ink transferred from an idealized gravure cell (also known as the pickout fraction) with increasing imposed extensional velocities, V_z, and shear velocities, V_x, was studied for the shear thickening fluid and compared to the results of a similar shear viscosity Newtonian fluid. The pickout behavior of this shear thickening fluid was previously studied for a purely extensional deformation through a combination of experiments and numerical simulations [37]. The pure extensional pickout measurements have been repeated here so they could be used for comparison with the measurements for both pure shear and mixed kinematics gravure printing experiments. The pickout fraction with increasing extensional velocity from 0.5 mm/s $\leq V_z \leq$ 200 mm/s is shown in Fig. 4 for both the shear thickening fluid and the Newtonian fluid. For velocities where the capillary number is low, the pickout is a quasi-equilibrium process and is governed predominantly by surface tension and gravity. As the velocity is increased, shear stresses become important and the effect of shear thickening becomes apparent. At low extensional velocities, $V_z < 3$ mm/s, the imposed extensional rate, $\dot{\epsilon} \cong V_z/L_i$, is not large enough to cause the extensional viscosity of the nanoparticle suspension to thicken. As a result it should behave like a Newtonian fluid in this regime and the pickout behavior of 13Si-PPG was found, as expected, to be similar to that of the Newtonian fluid. The lack of perfect collapse of the data in Fig. 4 are due to differences in shear viscosity between the nanoparticle suspension and the Newtonian silicon oil. If the data were plotted against capillary number instead of extensional velocity these data would collapse well.

At moderate extensional velocities, 3 mm/s $< V_z <$ 30 mm/s, the pickout fraction for 13S-PPG shown in Fig. 4 was found to grow rapidly from 0.4 to 0.7 with increasing velocity due to the onset of thickening of the fluid's extensional viscosity as seen in Fig. 3. Fil-

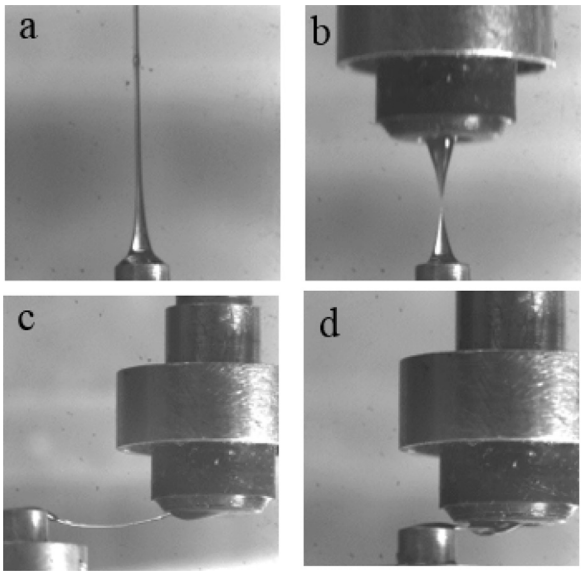

Fig. 5. Terminal filament interface profiles of 13Si-PPG for imposed extensional velocity of a) $V_z = 35$ mm/s, b) 80 mm/s, and shear velocity of c) $V_x = 7.5$ mm/s and (d) 25 mm/s.

ament stretching extensional rheology measurements have shown that the onset of thickening of the extensional viscosity occurs at extension rates of $\dot{\epsilon}_{cr} \sim \dot{\gamma}_{cr}/\sqrt{3}$. Where $\dot{\gamma}_{cr}$ is the critical shear rate for the onset of shear thickening which for the 13Si-PPG fluid was found to be $\dot{\gamma}_{cr} = 10\,s^{-1}$. This analysis is consistent for the onset of extensional thickening effects at $V_z = 3$ mm/s or an equivalent extension rate of $\dot{\epsilon}_{cr} \sim 4\ s^{-1}$. The large extensional viscosities of the 13Si-PPG solution in this regime are accompanied by long life times of the filaments pulled from the gravure cell as shown in the Fig. 5a. The stabilization of the fluid filaments against capillary breakup resulting from the large extensional viscosity of the fluid coupled with a break in the symmetry of the filament shape due to gravity has been shown through numerical simulations, to be the cause for the major pickout enhancement observed for shear thickening fluids [37]. In this case, the pickout fraction was found to double from 38% to 68%.

For large extensional velocities tested, $V_z > 30$ mm/s, the pickout fraction was found to quickly decline with increasing imposed velocity to less than 30% before reaching a plateau. In this regime, the fluid filaments were found to evolve from a uniform cylindrical shape at low deformation rates to a pair conical shaped filaments attached to the top and bottom end plates as shown in Fig. 5b. These conical shaped filaments were consistently observed within the high velocity plateau regime independent of the magnitude of the imposed velocity. The evolution of the conical shaped filament has been shown to be due to a sharp thinning of the shear and extensional viscosity of these fluids at large deformation rates [37]. By comparison, the pickout fraction obtained for the Newtonian fluid was found to decrease monotonically with increasing extensional velocity. This trend is consistent with the prediction of numerical simulations for Newtonian fluids, with the gravure cell on the top plate for Bond numbers greater than one [40]. The Bond number is the relative ratio of gravity to interfacial tension forces, $B_o = \rho g R^2/\sigma$ and is approximately $B_o \sim 3$ for the silicon oil tested here. The comparison with Newtonian fluid clearly demonstrates the dramatic impact shear thickening can have on gravure printing even in the absence of shear.

3.1.2. Effect of shear

The effect of a pure shear deformation on the pickout of the shear thickening fluid from an idealized gravure cell was studied by imposing a velocity orthogonal to the stretch direction, V_x, as seen in Fig. 1. The shear velocity was varied from 1 to 90 mm/s and the results are presented alongside the extensional pickout data in Fig. 4. At low shear velocities and capillary numbers, the pickout dynamics and fraction were predominantly governed by surface tension and gravity. The shear-induced pickout behavior of the Newtonian and shear-thickening fluid superimpose in this regime with both appear to be decreasing slightly with increasing shear velocity as expected from theory, experiments and simulations [13,31,41]. As the shear velocity was increased, the pickout fraction of each increased slowly. Small differences between the two fluids arose due to the fact that the viscosity and thus the capillary number of the Newtonian fluid is larger than the shear-thickening fluid at any given shear velocity in this flow regime as long as the shear rates are below critical shear rate for shear thickening, $\dot{\gamma} = V_x/L_i < \dot{\gamma}_{cr}$. As discussed previously, if the data were replotted as capillary number the Newtonian and shear thickening fluid data would superimpose in this regime. Slow growth in the pickout fraction is expected in this moderate capillary number regime, $Ca > 0.25$, as predicted by Campana and Carvalho [13].

For shear velocities ranging between 5 mm/s $< V_x <$ 7.5 mm/s, the shear-induced pickout of the shear-thickening fluids was found to increase quickly as a result of shear thickening. The shear rate at the onset of pickout enhancement was found to be approximately $\dot{\gamma} = V_x/L_i \sim 16 s^{-1}$. This corresponds well with the shear thickening transition observed in the rheological measurement in Fig. 2. Although the maximum pickout fraction was found to be much lower in shear than extension, 30% versus 70%, the changes resulting from the shear thickening transition still represents a 50% enhancement of the pickout fraction compared to the results from the low velocity regime. As shown in Fig. 5c, elongated filaments with significantly increased lifetimes were found to evolve at the late stages of the shear-induced pickout process at these velocities. These elongated filaments appeared after the plates had fully separated. As a result, even though the initially imposed flow kinematics were pure shear, once the plates fully separated, the flow transitioned to an extensional flow albeit in the x-direction. Because these stretches are not vertical, in some cases, sagging of the fluid filament under gravity can be observed.

With an increase in the shear velocity beyond $V_x > 7.5$ mm/s, the shear-induced pickout fraction exhibited a slow decline before eventually reaching a plateau at large shear velocities. In the plateau regime, the filaments were found to evolve from an elongated cylindrical filament towards a conical shape as shown in Fig. 5d. These filament shapes are similar to those observed in the plateau regime of the extensional pickout although aligned in the x-direction and distorted some by the shearing at the edge of the plates. This suggest a similar shear and extensional viscosity thinning transition of the viscosity can impact both shear-induced and extension-induced pickout dynamics. This observation is reinforced by the pickout fraction for the shear and extensional flow induced pickout which approach each other in the regime where conical filaments were formed.

In order to better understand the differences in the mechanism of shear and extensional pickout, the time evolution of shear and extensional pickout processes were examined through a high speed imaging. A sample time series for two experiments, a pure shear pickout and a pure extensional pickout with a velocity of $V_x = 7.5$ mm/s and $V_z = 10$ mm/s respectively are presented in Fig. 6. During the shear pickout process, at initial times when the horizontal displacement (x) of the bottom flat plate was within the width of the gravure cavity (D), $x < D$, the liquid bridge underwent a predominant shear deformation, where the liquid was dragged from the gravure cell onto the land outside the cell area. The instantaneous shear rate imposed by the top plate motion can be approximated as, $\dot{\gamma}_{xz} \sim V_x/L_i$. With time, the bottom flat plate

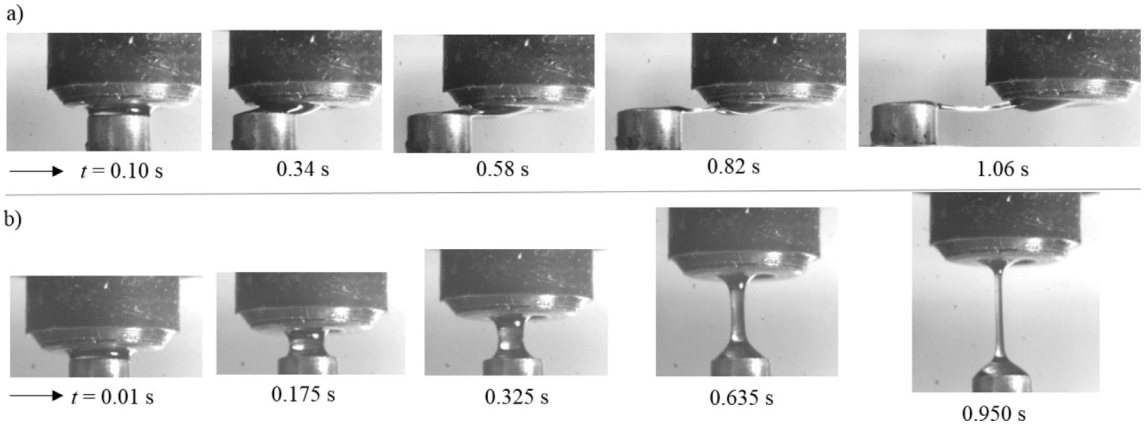

Fig. 6. Time evolution of a) pure shear-induced pickout at shear velocity of $V_x = 7.5$ mm/s and b) pure-extension-induced pickout at an extensional velocity of $V_z = 10$ mm/s for 13Si-PPG.

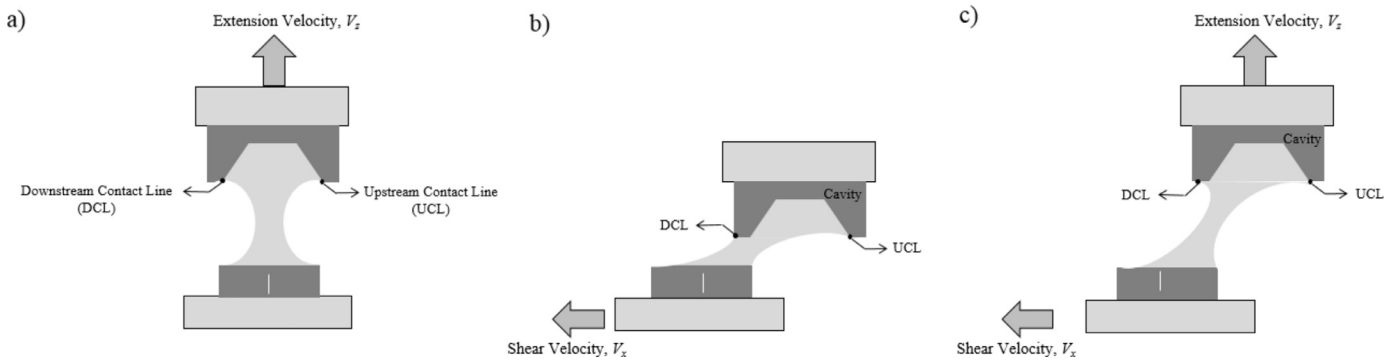

Fig. 7. Schematic diagram of a) pure extensional motion, b) pure shear motion and c) mixed shear and extension motion of an idealized gravure cell imposed during the liquid transfer process.

moved out from under the top plate ($x > D$). As this occurred, the shear flow is replaced by an elongational deformation, and the fluid on the cavity land is stretched until the breakup occurs. The late-stage evolution of shear-thickening filaments for pure shear-induced pickout at different velocities can be found in the bottom row of Fig. 9. It is clear from these images that the filament evolution due to late stage elongational stretching was present, even at the lowest shear velocity of $V_x = 1$ mm/s, after an initial shear deformation of the liquid bridge. The approximate transverse elongation rate after the plate separation, can be approximated as, $\dot{\gamma}_{xz} = V_x/X$, where $X = \sqrt{L_i^2 + (V_x t)^2}$ is the length of the filament. This transverse elongational rate decays with time because the imposed separation velocity is constant and eventually approaches $\dot{\gamma}_{xz} \propto 1/t$. The late stage filaments shapes and lengths formed during the shear pickout process were found to be quite similar to the filaments formed during extensional pickout, as shown in the first column of Fig. 9. The qualitative similarity between the trends of shear-induced pickout and the extensional-induced pickout is likely due to similar late stage extensional deformation and breakup dynamics of the filament seen in Fig. 9.

Given the late stage similarities, the reduction of the shear-induced pickout compared to the extensional-induced pickout is most likely due to the shearing of the liquid bridge at early times ($x < D$). At the early stages of the shear-induced pickout, the liquid from the gravure cell is forced to spread over the land bordering the gravure cavity. The formation of a static fluid reservoir on the cavity land driven out of the cavity by the shear deformation can be observed in the series of images in the bottom row of Fig. 9. This expansion of fluid wetting area could be major factor limiting the final shear-induced pickout fraction. This spreading of fluid onto cavity land in shear is shown schematically in the Fig. 7b and is absent in the extensional pickout out process due to axisymmetric stretching of the liquid bridge, as shown in the Fig. 7a. In the next section, we show that when an extension velocity is superimposed over shear, as shown in the Fig. 7c, this spreading of fluid onto the cavity land can be prevented, minimizing the loss of the pickout due to adhesion. Note, however, that the adhesion of the liquid in shear deformation and the resulting pickout loss could also be avoided by decreasing the wettability of the cavity land of the gravure cell through a physical and/or chemical pretreatment.

3.1.3. Effect of shear and extension

In this section, we present a study of the influence of a combination of the shear and extensional deformation on the total pickout of a shear-thickening fluid. In the experiments, four different shear velocities were chosen to superimpose over a wide range of extensional velocities ranging from $0.1 \leq V_z \leq 200$ mm/s. The pickout results for these experiments with complex flow kinematics are shown in Fig. 8. The fixed shear velocities were chosen from two shear pickout regimes; moderate velocities of $V_x = 5$ mm/s and 7.5 mm/s velocities, where the shear pickout exhibited an enhancement due to late stage transverse extensional thickening and large velocities of $V_x = 25$ mm/s and 80 mm/s, where the pickout plateaued due to shear and extensional thinning of the fluid. In the first regime, for fixed shear velocities of $V_x = 5$ mm/s and 7.5 mm/s, as the simultaneously-applied extensional velocity was increased, the total pickout fraction was found to increase from the pure shear pickout values up to and then beyond the value associated with the pure extensional pickout process. For the $V_x = 5$ mm/s case, the pure extension pickout fraction was improved by approximately 10% with the superposition of the shear veloc-

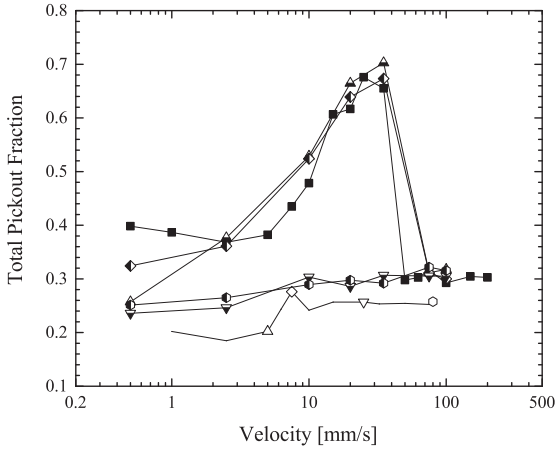

Fig. 8. Pickout fraction as a function of both extensional and shear velocities for 13Si-PPG. The data include for (filled diamond) pure extension and (hollow diamond) pure shear. Half-shaded symbols correspond to different fixed orthogonal velocities superimposed over varying extensional velocity. The shear velocities include: (△) $V_x = 5$ mm/s, (◇) 7.5 mm/s, (▽) 25 mm/s and (○) 80 mm/s.

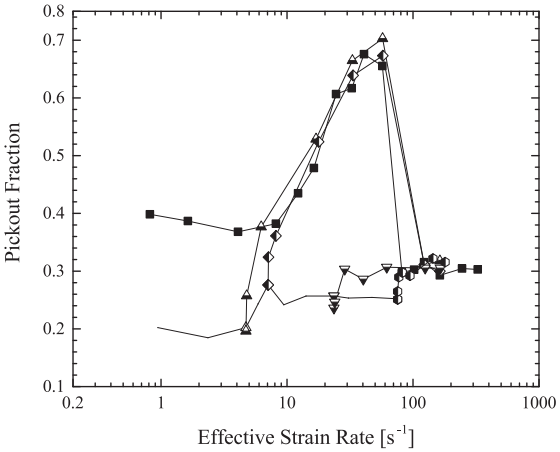

Fig. 10. Pickout fraction as a function of effective strain rate for 13Si–PPG. Filled symbols correspond to pure extension rate, $\dot{\gamma}_{zz} = \sqrt{3}\, V_z/L_i$ and hollow symbols correspond to pure shear rate, $\dot{\gamma}_{xz} = V_x/L_i$. The half-shaded symbols correspond to effective strain rate, $\dot{\gamma}_e = \sqrt{\frac{\dot{\gamma}_{xz}^2+\dot{\gamma}_{zz}^2}{2}}$.

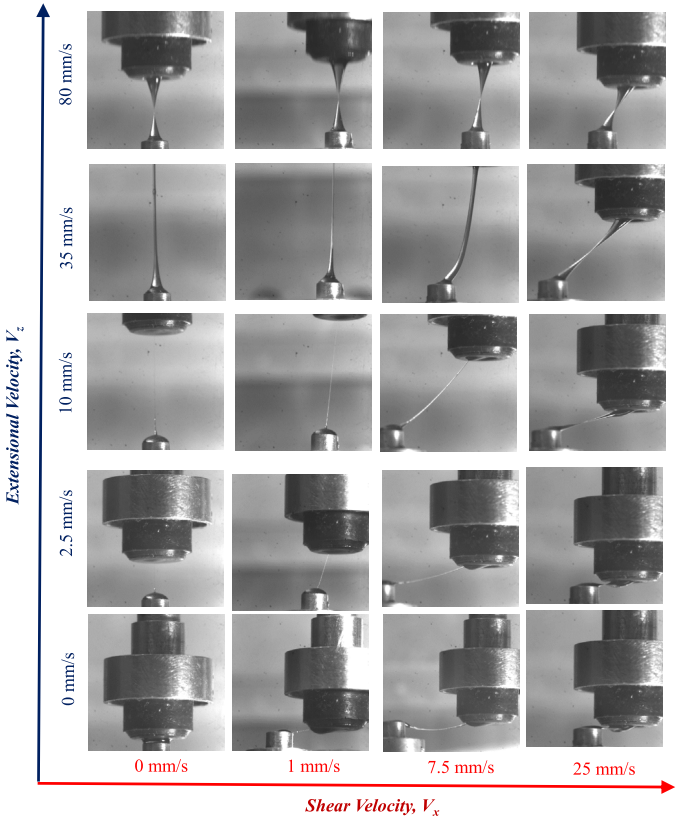

Fig. 9. Filament interface profiles just prior to break up for the shear thickening test fluid, 13Si-PPG , for a combination of imposed extensional velocities and shear velocities.

ity. This observed enhancement could be in part due to enhanced dewetting from the upstream gravure cell cavity corner as pictured in Fig. 7c.

The evolution in pickout behavior from shear dominated to extensionally dominated can be seen in the images of the final filament shape presented in Fig. 9. For shear velocities below $V_x <$ 7.5 mm/s, the terminal filament shapes gradually approach the shape of pure extensional pickout as the strength of the extensional flow is increased. Note, however, that the stretch orientation in each case becomes aligned with the direction of the total velocity vector. Interestingly, for larger superimposed shear velocities of $V_x = 10$ mm/s and 40 mm/s, as the extensional velocity was increased, the total pickout was found to increase only slightly before collapsing onto the high velocity terminal plateau value associated with pure extensional-induced pickout. As can be observed in Fig. 9, at these velocity combinations the filaments were found to consistently evolve into the conical shaped filaments associated with the onset of extensional thinning of the fluid at large extension rates [37].

This observation suggests that the data could be better understood if the relative strength of the shear and extensional deformation on the fluid pickout were not shown as velocities, but instead cast as an effective strain rate, $\dot{\gamma}_e = \sqrt{\frac{\dot{\underline{\gamma}}:\dot{\underline{\gamma}}}{2}} = \sqrt{\frac{\dot{\gamma}_{xz}^2+\dot{\gamma}_{zz}^2}{2}}$, where $\dot{\gamma}_{xz} = V_x/H$ and $\dot{\gamma}_{zz} = \sqrt{3}V_z/H$. The results are presented in Fig. 10. In Fig. 10, the pickout fraction for a combination of shear and extensional deformation collapses quite well when plotted against effective strain rate. The total pickout transitions from shear dominant to extensional dominant or vice-versa, can be clearly discriminated and it typically occurs once $\dot{\gamma}_{zz} > \dot{\gamma}_{xz}$. For the cases where the effective strain rates imposed were below the high extensional velocity plateau ($\dot{\gamma}_{xz} < 12$ s^{-1}), the total pickout was found to improve by approximately 10% for any given effective strain rate with the addition of even the smallest amount of shear. This improvement in the total pickout could be due to an effective dewetting of the upstream contact line down the cavity wall induced by the combination of shear and the extensional motion imposed. Although it should be noted that, even after making several attempts to visualize the contact line motion, experimental challenge made it impossible to collect any conclusive evidence for or against complete dewetting. What appears to be dewetting along the upstream corner of the gravure cell could simply be a large deformation of the fluid interface into the gravure cell while the contact line remained pinned at the upstream corner. We continue to explore new visualization techniques of the contact line motion in hopes of eventually being able to provide new insights on the mechanism of the ink transfer that can be utilized in future theoretical and computational studies.

The pickout fraction in Fig. 10 showed the same collapsed with increasing deformation rate as was observed pickout data for pure extension. However, it should be noted that, for the highest shear rates tested, $\dot{\gamma}_{xz} > 12$ s^{-1}, the superposition of additional extensional deformation only resulted in a slight increase in the pickout

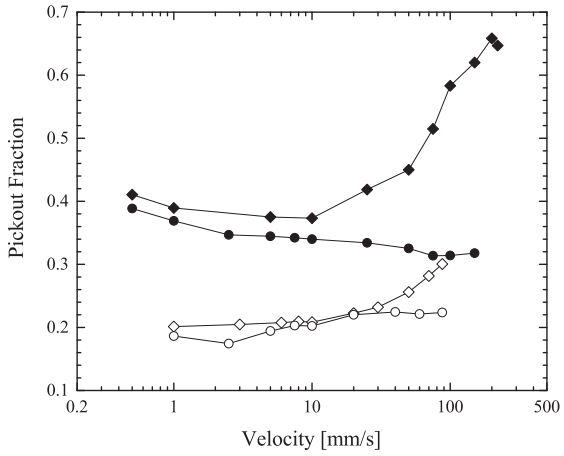

Fig. 11. Pickout fraction as a function of extensional velocity (filled symbols) and shear velocity (hollow symbols). The data include: (◊) 8M PEO and (•) silicone oil.

fraction. In these cases, the total pickout did not follow the trend in extensional pickout fraction even when the extension rates imposed were much larger than the imposed shear rates, $\dot{\gamma}_{zz} > \dot{\gamma}_{xz}$. Instead the pickout fraction variation with deformation rate was similar to the pure shear result. In all cases, when the effective strain rate is larger than $\dot{\gamma}_e > 90\ s^{-1}$ a plateau in the total pickout fraction was observed, accompanied by a conical filament profile as shown in Fig. 9. These results clearly demonstrate the importance of both late stage extensional deformation and the initial shear deformation on the pickout process in gravure printing. They also validate the use of the effective strain rate for physically interpreting the data as nearly all the data collapsed onto a single master curve when recast in this way.

3.2. Ink transfer behavior of a viscoelastic fluid

3.2.1. Effect of extension

The effect of shear and extensional deformation on the pickout behavior of viscoelastic fluids was also studied in order to extend these observations to a second class of non-Newtonian fluids. The pickout fraction with pure extensional velocities or pure shear velocities imposed between $0.1\ \text{mm/s} < V < 200\ \text{mm/s}$ are presented in Fig. 11. The data for the Newtonian silicone oil is also presented for comparison. The effect of extensional deformation on the pickout behavior of viscoelastic fluids was found to be consistent with the previous studies [10]. The extensional pickout was found to strongly increase, by more than 71%, with increasing velocity from 10 mm/s to 200 mm/s from a value of 38% to 65%. By comparison, at these high velocities, the pickout fraction of the viscoelastic solution was more than twice the Newtonian silicone oil. At low velocities, the Weissenberg number, $Wi = \lambda_E \dot{\epsilon} << 1$, is small. As a result, elastic effects are not important and, as expected, the data collapsed onto the results for the Newtonian fluid. The slight difference is due to the different in viscosity at these shear rate; the viscosity of the Newtonian fluid is significantly larger than the viscoelastic fluid. If the data were replotted as a function of capillary number instead of velocity, the Newtonian fluid data would shift to the right by a factor of more than ten and the data for both the fluids would collapse. At larger velocities, where the Weissenberg number is greater than one, $Wi > 1$, elastic effects become important resulting in the large deviation from the Newtonian result. As shown in first column of Fig. 13, the filaments were found to exhibit an increased lifetime for $V_z > 10$ mm/s because of the thickening of the extensional viscosity of the fluid. As described in the literature, the late stage break-up of the elongated filament near the top cavity and the subsequent gravitational drainage towards the bottom plate results in the enhancement of the extensionally-induced pickout [10,40].

3.2.2. Effect of shear

The effect of pure shear deformation on the fluid pickout is shown in Fig. 11. The pickout fraction of the viscoelastic fluid was found to increase slowly with increasing shear velocity up to a velocity of $V_x = 20$ mm/s much like the Newtonian. Beyond $V_x > 20$ mm/s, a sharp growth in the pickout fraction was observed within less than a decade change of 43% in imposed shear velocity. Over the same range of imposed shear velocities, the pickout fraction for the Newtonian fluid increased by only 10%. This behavior qualitatively matches the fluid response of pure extensional pickout although the viscoelastic enhancement in the shear-induced pickout fraction was slightly less dramatic. As shown in the bottom row of Fig. 13, with increasing shear velocity, the filament shape just prior to breakup were found to become more elongated in the transverse direction with increasing shear velocity. The filaments were also observed to survive longer before breakup. This observation suggests there is a thickening of the extensional viscosity of the fluid at late stages of the shear pickout process where the pickout process morphs from a shear to a extensional flow in the x-direction.

In the computational study performed by Chung and Kumar [43] for viscoelastic fluids, the presence of shear motion, for both the boundary condition with a pinned contact line at the top plate as well as with no free interface at the downstream (outlet) of the top plate, a growth in the normal stress at the top-corner of the cavity was found to enhance the pickout fraction. In our experiments, a similar pickout enhancement associated with a shear induced normal stress growth in the cavity corner in the initial shear motion is likely. Conversely, in the pure extensional motion, the computations by Lee et al. [40] on viscoelastic fluids show that such growth of the elastic normal stresses growth at the free surface near the cavity, albeit axisymmetric, were observed to hinder the fluid pickout at the initial times, however, the late stage filament dynamics were found to dominate the final pickout. One should note that although pickout fraction is improved with increasing shear velocity, the resulting elongated fluid filaments and the misalignment between the top and bottom plates at breakup will likely result in a significantly reduced printing fidelity as the shear velocity is increased. Although printing quality is not quantified here, the presence of horizontal, highly stretched filaments is clearly not desired in most real world gravure printing applications.

3.2.3. Effect of shear and extension

Finally, we examined the influence of a combination of shear and extensional deformation on the pickout fraction of the viscoelastic fluids (8M PEO). The pickout fraction with increasing extensional velocity for a series of four different shear velocities is superimposed over the extensional flow data in Fig. 12. At low extensional velocities where shear effects dominate, the pickout fraction was found to be close to, but always slightly larger than, the pure shear-induced pickout fractions. As the extensional velocity was increased, the pickout fraction was found to increase and approach the values of pure extensional pickout, eventually mirroring the pure extensional pickout data for extensional velocities above $V_x > 10$ mm/s. At these extensional velocities, the effects of strain hardening of the fluid's extensional viscosity to become dominant as seen from the long-lived filaments formed in Fig. 13. An enhancement in the total pickout fraction when an extensional motion is superimposed over horizontal motion has also been reported for numerical simulations of viscoelastic fluids [43].

The filament shapes just prior to breakup can be seen in Fig. 13 for a wide range of combinations of extensional and shear

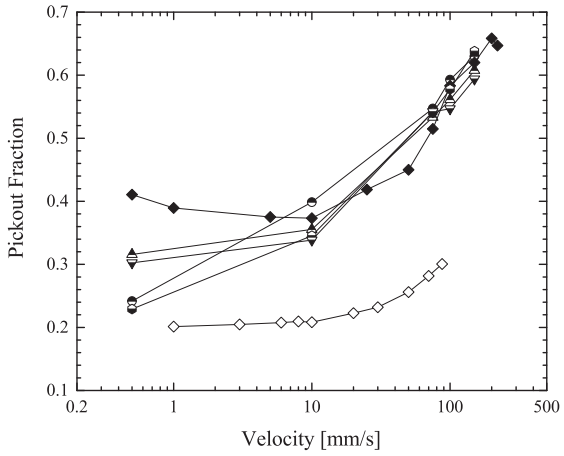

Fig. 12. Pickout fraction as a function of extensional and shear velocities for the viscoelastic test fluid, 8M PEO. The data include for (filled diamond) pure extension and (hollow diamond) pure shear. Half-shaded symbols correspond to different fixed shear velocities superimposed over varying extensional velocity. The superimposed shear velocities include: (△) $V_x = 1$ mm/s, (◯) 10 mm/s, (⬭) 30 mm/s and (▽) 80 mm/s.

velocities imposed. The filament were found to grow longer with increasing effective deformation rate and appear to dewet from the upstream gravure cavity corner with even the smallest amount of shear superimposed over the extensional flow. At high shear velocities, however, the filament appeared to be driven past the downstream corner and onto the land surrounding the gravure cell cavity. This could explain why at moderate imposed shear velocities, $V_x \leq 30$ mm/s the pickout fraction appears to be improved by 5 - 8% with the addition of shear, but at large shear velocities, $V_x \geq 80$ mm/s, shear appears to be slightly detrimental to the pickout fraction.

The effect of shear and extensional deformation on the fluid pickout can be made clearer if, as before, were cast the data as a function of the effective strain rate. This is done in Fig. 14. For the cases where both shear and extensional deformation were superimposed, a clear transition from a shear-dominated to an extension-dominated response can be observed as the imposed extensional strain rate grows larger than the imposed shear rate, $\dot{\gamma}_{zz} > \dot{\gamma}_{xz}$. This result reinforces the importance of considering the local shear and extension rates of the imposed flow in order to fully understand and predict the effect of process parameter variation on gravure printing of non-Newtonian liquids.

In this study we have examined the ink transfer behavior only for a cavity-on-top configuration for both shear thickening and viscoelastic fluids as mentioned previously. In the previous studies by our group [10,37] on the ink transfer behavior for an extensional deformation imposed using the same test fluids, the role of gravity on the pickout has been examined for both cavity-on-top and cavity-on-bottom configurations, as the Bond number of both viscoelastic fluids and the shear thickening fluids are $Bo \geq 1$. The fluid pickout was found to be assisted by gravity for a cavity-on-top configuration and a vice-versa effect for a cavity-on-bottom configuration, with marked effect at velocities where the fluid undergoes extensional thickening. The pickout study for an imposed shear

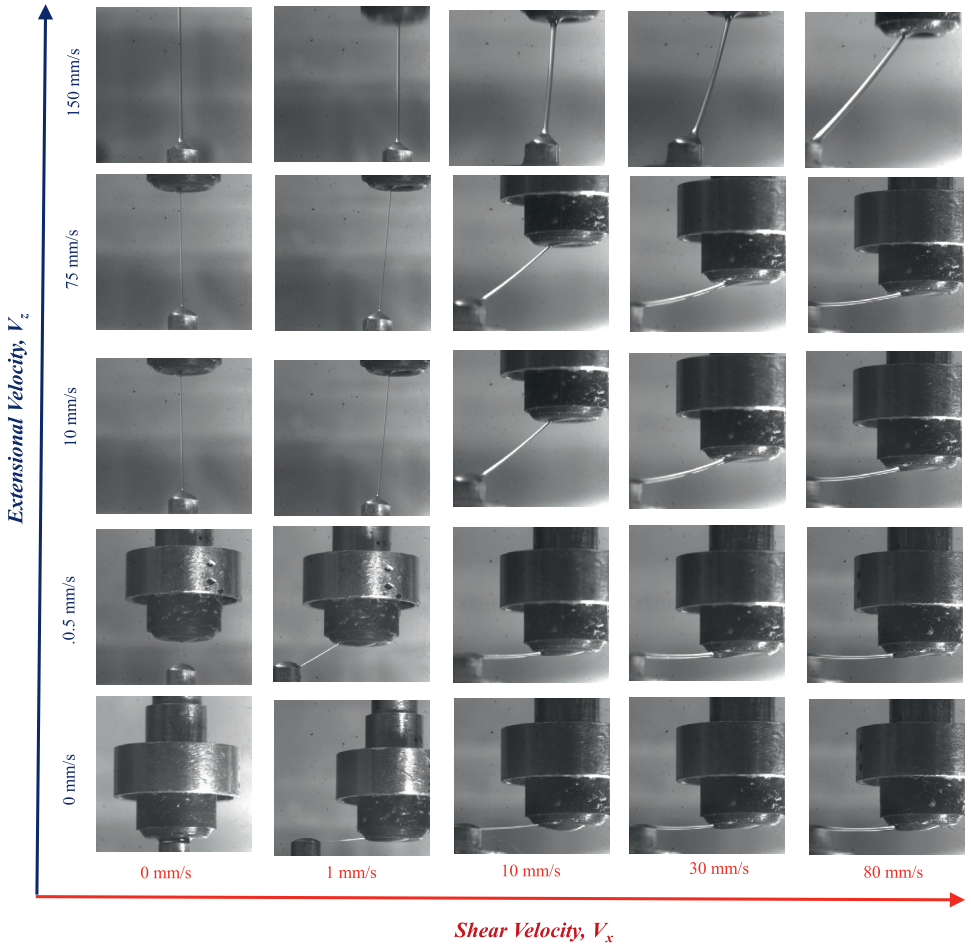

Fig. 13. Terminal filament interface profiles of 8M PEO for a combination of imposed extensional velocities and orthogonal velocities.

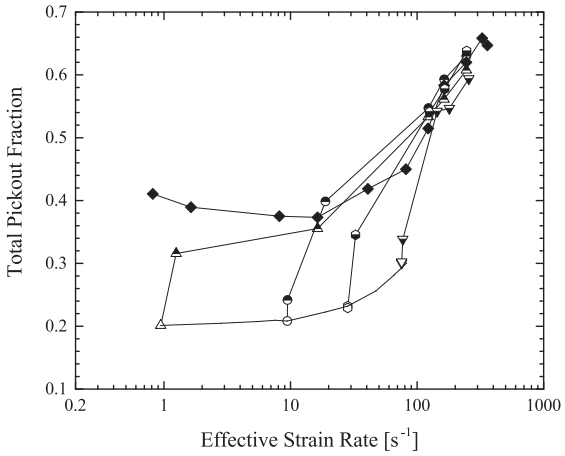

Fig. 14. Pickout fraction as a function of effective strain rate for the viscoelastic test fluid, 8M PEO. Filled symbols correspond to pure extension rate, $\dot{\gamma}_{zz} = \sqrt{3}\ V_z/L_i$ and hollow symbols correspond to pure shear rate, $\dot{\gamma}_{xz} = V_x/L_i$. The half-shaded symbols correspond to effective strain rate, $\dot{\gamma}_e = \sqrt{\frac{\dot{\gamma}_{xz}^2+\dot{\gamma}_{zz}^2}{2}}$.

deformation, with cavity-on-bottom configuration, which was not presented due to experimental difficulties, we expect gravity to have a similar negative effect on the shear pickout.

4. Conclusions

The impact of shear and extensional deformation on the liquid bridge during ink transfer from an idealized gravure cell was studied. The study was conducted for two different non-Newtonian fluids; one a shear-thickening nanoparticle dispersions and the other a constant shear viscosity viscoelastic polymer solution. The pickout dynamics were studied over a range of extensional and shear velocities chosen to induced shear thickening and elastic effects in the two fluids. With the imposition of a pure extensional pickout process, the shear-thickening fluid was found to initially behave like a Newtonian fluid before growing quickly, by 86%, with increasing imposed velocity. The growth in pickout fraction resulted from the extensional thickening for the fluid and the growth of highly elongated fluid filaments pulled from the gravure cells. At large velocities, the pickout fraction strongly decayed, by a factor of approximately two, due to the dramatic thinning of extensional viscosity of these fluids at large extension rates. The result was the formation of conical-shaped fluid filaments.

The shear-induced pickout behavior of shear-thickening fluids was found to be qualitatively similar to that of extension-induced pickout, however, the amplitude of the growth and decay of the pickout fraction was significantly weaker. The observation of evolution of the fluid filament shapes during the shear pickout indicated a late stage transverse from a shear to an extensional deformation process, with the filaments evolving with similar shapes to those observed during the extensional pickout process albeit aligned horizontally rather than vertically. However, the shear-induced pickout fraction was found to be significantly lower than the extensional pickout for a given velocity. The comparison of the time evolution of filaments suggested the weaker shear-induced pickout fraction is due to the shearing motion of the liquid bridge which pulls the fluid from the gravure cell and forces it onto the land bordering the gravure cavity. The increased liquid solid contact area increased the adhesion strength and limited the final pickout fraction. This adhesion of the liquid in shear deformation and the resulting pickout loss could be avoided and the pickout fraction can be increased by decreasing the wettability of the land through a physical/chemical pretreatment.

The effect of a combination of shear and extensional deformation on the pickout fraction of the shear thickening fluid was also studied. Superimposing extensional flow over shear improved the pickout fraction preventing the adhesion of the fluid onto gravity land area and eventually dominated by extensional deformation for $\dot{\gamma}_{zz} > \dot{\gamma}_{xz}$. For shear velocity below the rate-thinning pickout plateau regime, superimposing extensional velocities was found improve the pickout fraction for up to 10%, which is likely associated with asymmetric dewetting of the upstream cavity wall by the superimposed flow. Whereas for a shear velocity in the rate-thinning plateau regime, superposition of extensional velocities only exhibited a slight enhancement in the pickout fraction. The effect of shear and extensional deformation on the pickout fraction was further examined by casting the pickout data as a function of effective strain rate. The transitions of the pickout behavior from shear to extension-dominated deformation regimes or vice-versa were clearly observed as a function of strain rate.

For the case of viscoelastic fluids, the extension-induced pickout was found to exhibit a strong increase with increasing velocity, up to 71%, compared to a Newtonian fluid. This enhancement in the pickout fraction is due to the extensional thickening of the fluid, accompanied by a long-lived fluid filaments for Weissenberg number greater than one, $Wi > 1$. The shear-induced pickout exhibited a similar growth, by 43%, with increasing shear velocity. The enhancement in the shear-induced pickout is due to the late stage elongation deformation transversed from pure shear after the plates were fully separated and the resulting thickening of the extensional viscosity. This is further confirmed from the observation of the long uniform filaments with increased life-time similar to observed in the extension-induced pickout process. As before, the shear-induced pickout magnitude was found to significantly lower than that of the extension-induced pickout.

The influence of a combination of shear and extensional deformation on the pickout fraction was also studied for the viscoelastic fluids. Superimposing a small extensional velocity on a predominantly shear flow improved pickout fraction by avoiding adhesion of the pickout on the gravure cavity land. Superimposing of extensional velocities over moderate shear velocity improved the total pickout fraction by roughly 5 - 8%. This increase could be due in some part to the enhanced interface deformation and perhaps even dewetting of the fluid at the upstream corner of the gravure cell due to the symmetry breaking effects of the added shear. Whereas at large shear velocities, superimposing extensional velocities was found to be reduce the pickout fraction by approximately 6%. When the pickout fraction is presented not as function of velocity but as a function of effective strain rate the data collapsed onto a single master curve. Using the effective strain rate a clear transition was observed between shear and extensional dominated response for $\dot{\gamma}_{zz} > \dot{\gamma}_{xz}$ during the ink transfer process.

Acknowledgments

The authors would like to thank National Science of Foundation for funding the current project through the Center For Hierarchical Manufacturing at UMASS under grant number CMMI-1025020.

References

[1] R.R. Søndergaard, M. Hösel, F.C. Krebs, Roll-to-roll fabrication of large area functional organic materials, J. Polym. Sci. Part B 51 (1) (2013) 16–34.
[2] A. Hübler, B. Trnovec, T. Zillger, M. Ali, N. Wetzold, M. Mingebach, A. Wagenpfahl, C. Deibel, V. Dyakonov, Printed paper photovoltaic cells, Adv. Energy Mater. 1 (6) (2011) 1018–1022.
[3] W. Yue, T.T. Larsen-Olsen, X. Hu, M. Shi, H. Chen, M. Hinge, P. Fojan, F.C. Krebs, D. Yu, Synthesis and photovoltaic properties from inverted geometry cells and roll-to-roll coated large area cells from dithienopyrrole-based donor-acceptor polymers, J. Mater. Chem. A 1 (2013) 1785–1793.
[4] F.C. Krebs, T. Tromholt, M. Jørgensen, Upscaling of polymer solar cell fabrication using full roll-to-roll processing, Nanoscale 2 (2010) 873–886.

[5] M. Hösel, F.C. Krebs, Large-scale roll-to-roll photonic sintering of flexo printed silver nanoparticle electrodes, J. Mater. Chem. 22 (2012) 15683–15688.
[6] L. Gonzalez-Macia, A. Morrin, M.R. Smyth, A.J. Killard, Advanced printing and deposition methodologies for the fabrication of biosensors and biodevices, Analyst 135 (2010) 845–867.
[7] C.F. Huebner, J.B. Carroll, D.D. Evanoff, Y. Ying, B.J. Stevenson, J.R. Lawrence, J.M. Houchins, A.L. Foguth, J. Sperry, S.H. Foulger, Electroluminescent colloidal inks for flexographic roll-to-roll printing, J. Mater. Chem. 18 (2008) 4942–4948.
[8] A.M. Almanza-Workman, C.P. Taussig, A.H. Jeans, R.L. Cobene, Fabrication of three-dimensional imprint lithography templates by colloidal dispersions, J. Mater. Chem. 21 (2011) 14185–14192.
[9] G. Hernandez-Sosa, N. Bornemann, I. Ringle, M. Agari, E. Dörsam, N. Mechau, U. Lemmer, Rheological and drying considerations for uniformly gravure-printed layers: Towards large-area flexible organic light-emitting diodes, Adv. Funct. Mater. 23 (2013) 3164.
[10] A.K. Sankaran, J.P. Rothstein, Effect of viscoelasticity on liquid transfer during gravure printing, J. Non-Newtonian Fluid Mech. 175–176 (2012) 64–75.
[11] H. Kang, R. Kitsomboonloha, J. Jang, V. Subramanian, High-performance printed transistors realized using femtoliter gravure-printed sub-10 µm metallic nanoparticle patterns and highly uniform polymer dielectric and semiconductor layers, Adv. Mater. 24 (22) (2012) 3065–3069.
[12] M.M. Voigt, A. Guite, D.-Y. Chung, R.U.A. Khan, A.J. Campbell, D.D.C. Bradley, F. Meng, J.H.G. Steinke, S. Tierney, I. McCulloch, H. Penxten, L. Lutsen, O. Douheret, J. Manca, U. Brokmann, K. Sönnichsen, D. Hülsenberg, W. Bock, C. Barron, N. Blanckaert, S. Springer, J. Grupp, A. Mosley, Polymer field-effect transistors fabricated by the sequential gravure printing of polythiophene, two insulator layers, and a metal ink gate, Adv. Funct. Mater. 20 (2) (2010) 239–246.
[13] D.M. Campana, M.S. Carvalho, Liquid transfer from single cavities to rotating rolls, J. Fluid Mech. 747 (2014) 545–571.
[14] S. Kumar, Liquid transfer in printing processes: Liquid bridges with moving contact lines, Ann. Rev. Fluid Mech. 47 (1) (2015) 67–94.
[15] M. Pudas, S. Leppavuori, J. Hagberg, The absorption ink transfer mechanism of gravure offset printing for electronic circuitry, in: IEEE Transactions on Electronics Packaging Manufacturing, vol. 25, 2002, pp. 335–343.
[16] B. Qian, K.S. Breuer, The motion, stability and breakup of a stretching liquid bridge with a receding contact line, J. Fluid Mech. 666 (2011) 554–572.
[17] D. Rivas, J. Meseguer, One-dimensional self-similar solution of the dynamics of axisymmetric slender liquid bridges, J. Fluid Mech. 138 (1984) 417–429.
[18] S. Gaudet, G.H. McKinley, H.A. Stone, Extensional deformation of Newtonian liquid bridges, Phys. Fluids 8 (10) (1996) 2568–2579.
[19] R.D. Gillette, D.C. Dyson, Stability of fluid interfaces of revolution between equal solid circular plates, Chem. Eng. J. 2 (1) (1971) 44–54.
[20] J. Meseguer, The breaking of axisymmetric slender liquid bridges, J. Fluid Mech. 130 (1983) 123–151.
[21] L. Rayleigh, On the instability of jets, Proc. London Math. Soc. 10 (1878) 4–13.
[22] J.A.F. Plateau, Experimental and Theoretical Researches on the Figures of Equilibrium of a Liquid Mass Withdrawn from the Action of Gravity, Annual Report of the Board of Regents and Smithsonian Institution, Washington, DC, 1863, pp. 2568–2579.
[23] H.W. Kang, H.J. Sung, T.-M. Lee, D.-S. Kim, C.-J. Kim, Liquid transfer between two separating plates for micro-gravure-offset printing, J. Micromech. Microeng. 19 (2009) 015025.
[24] P.P. Bhat, O.A. Basaran, M. Pasquali, Dynamics of viscoelastic liquid filaments: low capillary number flows, J. Non-Newton. Fluid Mech. 150 (23) (2008) 211–225.
[25] P.P. Bhat, S. Appathurai, M.T. Harris, M. Pasquali, G.H. McKinley, O.A. Basaran, Formation of beads-on-a-string structures during break-up of viscoelastic filaments, Nat. Phys. 6 (8) (2010) 625–631.
[26] C.-H. Huang, M.S. Carvalho, S. Kumar, Stretching liquid bridges with moving contact lines: comparison of liquid-transfer predictions and experiments, Soft Matter 12 (2016) 7457–7469.
[27] C.A. Powell, M.D. Savage, J.T. Guthrie, Computational simulation of the printing of newtonian liquid from a trapezoidal cavity, Int. J. Numer. Methods Heat Fluid Flow 12 (2002) 338–355.
[28] S. Dodds, M. da Silveira Carvalho, S. Kumar, Stretching and slipping of liquid bridges near plates and cavities, Phys. Fluids 20 (2009) 092103.
[29] S. Dodds, M. da Silveira Carvalho, S. Kumar, Stretching liquid bridges with moving contact lines: the role of inertia, Phys. Fluids 23 (2011) 092101.
[30] W.-X. Huang, S.-H. Lee, H.J. Sung, T.-M. Lee, D.-S. Kim, Simulation of liquid transfer between separating walls for modeling micro-gravure-offset printing, Int. J. Heat and Fluid Flow 29 (5) (2008) 1436–1446.
[31] X. Yin, S. Kumar, Flow visualization of the liquid-emptying process in scaled-up gravure grooves and cells, Chem. Eng. Sci. 61 (2006) 1146–1156.
[32] X. Yin, S. Kumar, Lubrication flow between a cavity and a flexible wall, Phys. Fluids 17 (2005) 063101.
[33] C.A. Powell, M.D. Savage, P.H. Gaskell, Modelling the meniscus evacuation problem in direct gravure coating, Chem. Eng. Res. Des. 78 (1) (2000) 61–67.
[34] N. Hoda, S. Kumar, Boundary integral simulations of liquid emptying from a model gravure cell, Phys. Fluids 20 (2008) 092106.
[35] S. Dodds, M.S. Carvalho, S. Kumar, The dynamics of three-dimensional liquid bridges with pinned and moving contact lines, J. Fluid Mech. 707 (2012) 521–540.
[36] M.A. Johnson, Viscoelastic Roll Coating Flows., University of Maine, 2003 Ph.D. thesis.
[37] S. Khandavalli, J.A. Lee, M. Pasquali, J.P. Rothstein, The effect of shear-thickening on liquid transfer from an idealized gravure cell, J. Non-Newtonian Fluid Mech. 221 (2015) 55–65.
[38] F. Ghadiri, D.H. Ahmed, H.J. Sung, E. Shirani, Non-newtonian ink transfer in gravure-offset printing, Int. J. Heat and Fluid Flow 32 (2011) 308–317.
[39] S. Ahn, S. Lee, Y. Na, Elasticity effect on the ink transfer process in gravure printing, in: Computational Science and Its Applications, 2008, pp. 565–575.
[40] J.A. Lee, J.P. Rothstein, M. Pasquali, Computational study of viscoelastic effects on liquid transfer during gravure printing, J. Non-Newtonian Fluid Mech. 199 (2013) 1–11.
[41] H.-K. Chuang, C.-C. Lee, T.-J. Liu, An experimental study on the pickout of scaled-up gravure cells, Int. Polym. Proc. 2 (2008) 216–222.
[42] C.-C. Lee, S.-H. Hu, T.-J. Liu, C. Tiu, Three-dimensional observation on the liquid emptying process from a scaled-up gravure cell, Int. Polym. Proc. 1 (2012) 128–137.
[43] C. Chung, S. Kumar, Emptying of viscoelastic liquids from model gravure cells, J. Non-Newton. Fluid Mech. 221 (2015) 1–8.
[44] S.R. Raghavan, S.A. Khan, Shear-induced microstructural changes in flocculated suspensions of fumed silica, J. Rheol. 39 (6) (1995) 1311–1325.
[45] F.J. Galindo-Rosales, Static and dynamic yield stresses of aerosil® 200 suspension in polypropylene glycol, Appl. Rheol. (2010).
[46] N.J. Wagner, J.F. Brady, Shear thickening in colloidal dispersions, Phys. Today 62 (10) (2009) 27–32.
[47] V.M. Entov, E.J. Hinch, Effect of a spectrum of relaxation times on the capillary thinning of a filament of elastic liquid, J. Non-Newtonian Fluid Mech. 72 (1997) 31–53.
[48] A. Bhardwaj, E. Miller, J.P. Rothstein, Filament stretching and capillary breakup extensional rheometry measurements of viscoelastic wormlike micelle solutions, J. Rheol. 51 (4) (2007) 693–719.
[49] L.E. Rodd, T.P. Scott, J.J. Cooper-White, G.H. McKinley, Capillary break-up rheometry of low-viscosity elastic fluids, Appl. Rheol. 15 (1) (2005) 12–27.
[50] S.L. Anna, G.H. McKinley, Elasto-capillary thinning and breakup of model elastic liquids, J. Rheol. 45 (1) (2001) 115–138.
[51] D.T. Papageorgiou, On the breakup of viscous liquid threads, Phys. Fluids 7 (1995) 1529–1544.
[52] O. Arnolds, H. Buggisch, D. Sachsenheimer, N. Willenbacher, Capillary breakup extensional rheometry (CaBER) on semi-dilute and concentrated polyethyleneoxide (PEO) solutions, Rheol. Acta 49 (11) (2010) 1207–1217.